Macromolecules
ARTICLE

Macromolecules **2009**, *42*, 8661–8668 **8661**
DOI: 10.1021/ma9016604

Amphiphilic Polystyrene-*b*-poly(*p*-hydroxystyrene-*g*-ethylene oxide) Block−Graft Copolymers via a Combination of Conventional and Metal-Free Anionic Polymerization

Junpeng Zhao,[†,‡] Grigoris Mountrichas,[‡] Guangzhao Zhang,[†] and Stergios Pispas*[,‡]

[†]*Hefei National Laboratory for Physical Sciences at Microscale, University of Science and Technology of China, Hefei, Anhui, China, and* [‡]*Theoretical and Physical Chemistry Institute, National Hellenic Research Foundation, 48 Vassileos Constantinou Ave., 11635 Athens, Greece*

Received July 28, 2009; Revised Manuscript Received September 18, 2009

ABSTRACT: This work presents the synthesis of polystyrene-*block*-poly(*p*-hydroxystyrene-*graft*-ethylene oxide), PS-*b*-(PHOS-*g*-PEO), amphiphilic block−graft copolymers. The backbone diblock copolymers (PS-*b*-PHOS) were prepared by lithium-based anionic polymerization, followed by postpolymerization acid hydrolysis of the poly(*p*-*tert*-butoxystyrene), PtBOS, precursor block. The PEO side chains were synthesized by metal-free anionic ring-opening polymerization of ethylene oxide (EO), using the phosphazene base (*t*-BuP_4) and the phenolic hydroxyl groups (PhOH) in the backbones as the complex multifunctional initiating system. In all cases, starlike block−graft copolymers with high molecular weights and low polydispersities were synthesized. Well-controlled polymerization was achieved even with the molar ratio of *t*-BuP_4 to PhOH being equal to 0.2. Dynamic and static light scattering and fluorescence spectroscopy studies were carried out to investigate the solution behavior of the amphiphilic block−graft copolymers, including the critical micelle concentration and structural characteristics of the aggregates formed in aqueous solutions. Because of the high PEO content and the starlike macromolecular architecture, the PS-*b*-(PHOS-*g*-PEO) block−graft copolymers form highly swelled aggregates with low aggregation numbers, having nanostructures resembling hyperbranched clusters.

Introduction

Amphiphilic graft copolymers with poly(ethylene oxide) being the hydrophilic side chains have gained extensive academic interest in terms of both synthesis and physical properties.[1,2] Because of their unique behavior in terms of solubility, surface wetting, blood compatibility, and crystalline structure,[1−3] this kind of comblike or starlike copolymer has shown great potential in various significant applications, including drug delivery.[4]

The physical properties of PEO-based amphiphilic graft copolymers are greatly dependent on the molecular parameters, including the chemical nature and molecular composition of the hydrophobic backbone polymer, the length of the PEO side chains, and the grafting density.[1−4] Therefore, the development of such graft copolymers with different molecular architectures has been studied extensively during the past decade. In general, three synthetic methodologies can be found in the literature. The most widely utilized one is the macromonomer technique ("grafting through"), which involves almost all kinds of conventional polymerization methods, including cationic polymerization,[5] anionic polymerization,[6] ring-opening polymerization,[7,8] free radical polymerization,[9] nitroxide-mediated polymerization,[10] reversible addition−fragmentation chain transfer polymerization,[11] and atom transfer radical polymerization.[12,13] This technique usually gives graft copolymers with high grafting densities. However, due to the low activity of the macromonomer, the weight-average molecular weight (M_w) of PEO side chains is limited (M_w < 2000) in order to achieve good control of the polymerization and low polydispersity of the final graft copolymer. The second one is the "grafting to" technique, namely, the reaction of end-functionalized PEO with reactive groups on the backbone polymer.[14−16] The graft copolymers obtained by this technique usually have low grafting densities because of the high steric hindrance experienced by the tethered chains. Moreover, the length of the PEO side chains is also somewhat limited because of the low end-group reactivity and the slow kinetics of the reaction when high molecular weight tethered chains are involved. Finally, the multifunctional macroinitiator technique ("grafting from") has also been reported, although in a relatively smaller number of cases.[17−20] Potassium alkoxides are usually employed as the initiators for ethylene oxide (EO). The low steric hindrance and high activity of the EO monomer allow the realization of more tunable molecular architectures, with either high or low grafting density[18] and with either long or short PEO side chains.[17,18]

The phosphazene base *t*-BuP_4 has been used to generate effective counterions, either with lithium cation ($[t\text{-Bu}P_4\text{Li}]^+$)[21−23] or with proton ($[t\text{-Bu}P_4\text{H}]^+$),[24−26] for the anionic polymerization of EO. The primary advantage of using *t*-BuP_4 is that such a strong and bulky organic base leads to much softer counterions compared to metal cations, which favors higher polymerization rates, due to the counterion effect on the ion pair association and living end reactivity.[24,25] Moreover, the well-soluble $[t\text{-Bu}P_4\text{H}]^+$ cations improve the solubility of polyalkoxide initiator compared to metal-based polyalkoxides,[24] leading to more homogeneous reaction media, which in turn offers the possibility to synthesize well-defined PEO-based graft copolymers. To the best of the authors' knowledge, the only work reported on this *t*-BuP_4-based polyalkoxide initiating systems is that from Möller et al.[24] The poly[ethylene-*co*-(vinyl alcohol)]/*t*-BuP_4 combination was used as the multifunctional initiating system. However, the poor

*Corresponding author: Tel +30210-7273824; Fax +30210-7273794; E-mail pispas@eie.gr.

Published on Web 09/30/2009

Table 1. Molecular Characteristics of the Backbones and the Block−Graft Copolymers

sample	t-BuP_4/PhOH[a]	EO/P_b[b]	$M_{w,SEC}$[c] × 10^{-5} (g/mol)	M_w/M_n[c]	f_g[d] (%)	$M_{w,cal}$[e] × 10^{-5} (g/mol)	$M_{w,NMR}$[f] × 10^{-5} (g/mol)
SHOS1 (30.5 wt % PHOS)			0.18	1.14			
SHOS1gEO1	1.0	20	1.47	1.05	73.2	2.21	3.16
SHOS1gEO2	0.5	20	1.52	1.08	74.6	2.31	3.22
SHOS1gEO3	0.2	20	1.79	1.08	84.5	2.61	3.71
SHOS1gEO4	0.5	14.3	1.27	1.01	88.0	1.88	2.34
SHOS2 (44.8 wt % PHOS)			0.48	1.19			
SHOS2gEO1	0.5	21.8	6.62	1.20	89.5	9.28	11.6

[a] Molar ratio of t-BuP_4 to PhOH groups for each polymerization. [b] Feed ratio (w/w) of EO to the backbone for each polymerization. [c] By SEC. [d] Weight fraction of the block−graft copolymer in the crude reaction product (from SEC analysis). [e] Calculated by f_g and the known molecular weight of the backbone. [f] Calculated by the data of ^{1}H NMR with the known molecular weight of the backbone.

Scheme 1. General Synthetic Scheme for the Preparation of Polystyrene-*block*-poly(*p*-hydroxystyrene-*graft*-ethylene oxide) Copolymers

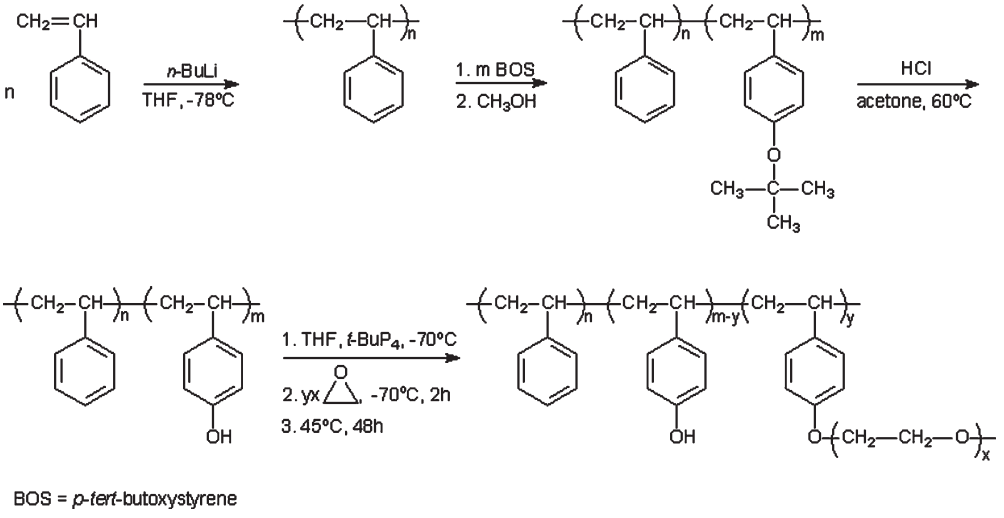

solubility and high polydispersity of the backbone copolymer were obstacles to the synthesis of well-defined graft copolymers. Thus, it seems necessary to utilize a more well-defined and well-soluble backbone polymer in order to investigate in detail the effect of this complex multifunctional initiating system on the graft polymerization of ethylene oxide, in an effort to synthesize well-defined amphiphilic macromolecules with complex architectures.

In this paper, we investigate the synthesis of PEO-based amphiphilic block−graft copolymers with $[t\text{-}BuP_4H]^+$ as the counterion, employing anionic polymerization high-vacuum techniques. Polystyrene-*block*-poly(*p*-hydroxystyrene) (PS-*b*-PHOS), which has good solubility in the reaction solvent (tetrahydrofuran), was utilized as the backbone copolymer to generate multifunctional initiators with t-BuP_4 coordination. These backbone block copolymers were prepared by post-polymerization hydrolysis of polystyrene-*block*-poly(*p*-*tert*-butoxystyrene) copolymers, which were synthesized via conventional anionic polymerization, utilizing *n*-BuLi as the organometallic initiator. Different experimental conditions were investigated for the graft polymerization of EO, with emphasis on varying the ratio of the two species comprising the initiating system (t-BuP_4/PhOH). The thermal and solution properties of the well-defined amphiphilic block−graft copolymers were also studied by differential scanning calorimetry, static and dynamic light scattering, and fluorescence spectroscopy.

Experimental Section

Polymer Synthesis. All reagents were purified by standard procedures followed routinely in anionic polymerization high-vacuum techniques.[27−29] The synthetic route for the preparation of the backbone diblock copolymer, PS-*b*-PHOS, and the block−graft copolymer, PS-*b*-(PHOS-*g*-PEO), is presented in Scheme 1. Typically, for the synthesis of SHOS1 (Table 1), the precursor diblock copolymer, polystyrene-*block*-poly(*p*-*tert*-butoxystyrene) (PS-*b*-PtBOS), was first prepared in tetrahydrofuran (THF, ∼150 mL) at −78 °C by sequential addition of styrene (10.0 g, 0.096 mol) and tBOS (6.5 g, 0.037 mol), where *n*-butyllithium (2.0×10^{-4} mol/mL in benzene, 5.2 mL) was used as the initiator and methanol (∼1 mL) as the terminator. The conversion of the monomers is 100%. After precipitation in methanol and drying in vacuum, the precursor diblock copolymer (5.0 g, 0.011 mol tBOS) was subjected to acidic hydrolysis in 5 wt % acetone solution at 60 °C, using 5-fold excess of hydrochloric acid (HCl) over the *tert*-butoxy groups.[28,29] The hydrolysis was continued for 6 h, and the final copolymer SHOS1, to be used as the backbone in subsequent synthesis steps, was isolated by precipitation into *n*-hexane. The yield of the hydrolysis is nearly 100%,[28,29] and the molecular characteristics of the backbone copolymers are listed in Table 1.

Block−graft copolymers were synthesized via metal-free anionic polymerization of ethylene oxide (EO) in THF, using PS-*b*-PHOS as the backbone and t-BuP_4−PhOH as the initiating system. Before each polymerization, the appropriate amount of backbone copolymer was purified by azeotropic distillation with THF,[17,18] left under high vacuum for 24 h, and finally dissolved again in dry THF, by use of a high-vacuum line. The synthesis of SHOS1gEO1 (Table 1) is presented in more detail as a typical example. Purified solvent (dry THF, ∼40 mL) was distilled into the polymerization apparatus, and the apparatus was degassed and flame-sealed. A predetermined amount of t-BuP_4 solution (1.0×10^{-4} mol/mL in benzene, 6.4 mL) was first added, giving the desired t-BuP_4/PhOH ratio, and the temperature was decreased to −70 °C. Subsequently, the THF solution of SHOS1 (0.25 g in ∼10 mL of THF, 6.4×10^{-4} mol of PhOH) was added via a break-seal to generate the

initiating system. The solution was stirred for 10 min at −70 °C before EO (5.0 g, 0.114 mol) was introduced by distillation. The reaction mixture was stirred at −70 °C for 2 h, then slowly heated to 45 °C, and stirred at this temperature for 48 h. The polymerization was terminated by addition of degassed methanol (∼1 mL) and a few drops of concentrated HCl.

After the polymerization, the solvent was evaporated in a rotary evaporator. The crude product was dried in vacuum overnight and weighed in order to determine the conversion of the monomer, which approached 100% in all cases. The crude product was purified by at least two fractionations, using chloroform as the solvent and *n*-hexane as the precipitant, in order to remove reaction byproducts, mainly PEO homopolymer. The molecular characteristics of the block−graft copolymers are listed in Table 1.

Characterization Methods. Size exclusion chromatography (SEC) and nuclear magnetic resonance (^{1}H NMR) were used to determine the molecular weights, compositions, and polydispersities of the copolymers. SEC determinations were performed on a Waters system equipped with a Waters 1515 pump, a Waters 2414 differential refractive index detector, and three μ-styragel columns with a continuous porosity of 10^2-10^5 Å. THF (with 5% v/v triethylamine) was used as the eluent, and the flow rate was 1.0 mL/min at 30 °C. The system was calibrated using a series of monodisperse linear polystyrene standards with weight-average molecular weights in the range of 2500−2 100 000 g/mol. ^{1}H NMR (300 MHz) spectra were recorded on a Bruker AC 300 instrument, operating at 300 MHz and at 25 °C, using chloroform-*d* ($CDCl_3$) as the solvent.

Differential scanning calorimetry (DSC) measurements were performed on a Q 200 modulated DSC from TA Instruments. The solid samples (∼4 mg) were loaded in aluminum pans. Standard DSC heating and cooling scans were performed at 10 °C/min under a helium atmosphere. The sample was cooled from room temperature to −150 °C. After an isothermal period of 10 min at −150 °C the sample was then heated to 150 °C in order to complete the first cycle. The second cycle was performed under the same extreme temperatures, after leaving the sample for 10 min at 150 °C. The data accumulated from the second heating cycle are reported here. Prior to use the calorimeter was calibrated with indium in respect to temperature and enthalpy changes.

For light scattering (LS) and fluorescence measurements, aqueous solutions at different concentrations of each block−graft copolymer were prepared by successive dilution of the stock solution, which was made either by directly dissolving a predetermined amount of the solid sample in water at 60 °C overnight or by adding the THF solution of the block−graft copolymer dropwise to water, followed by evaporation of THF (THF−water protocol). The second solution preparation protocol was followed for sample SHOS2gEO1 (Table 1), which was not soluble in water directly.

For the determination of the critical micelle concentration (cmc), by fluorescence spectroscopy, pyrene was added to the copolymer solutions at the concentration of 2.7×10^{-7} M. The solutions were then allowed to stay at room temperature overnight to achieve equilibrium. Fluorescence spectra were recorded on a Fluorolog-3, model FL3-21, Jobin Yvon-Spex spectrometer. Excitation wavelength was $\lambda = 335$ nm, and emission spectra were recorded in the region 350−500 nm, with an increment of 1 nm, using an integration time of 0.5 s. Slit openings of 1 mm were used for both the excitation and the emitted beams. The I_1/I_3 ratios were determined as the average of three measurements (where I_1 and I_3 are the intensities of the first and the third peaks of the pyrene fluorescence spectra at 372 and 383 nm, respectively). Copolymer concentrations were in the range of $1.0 \times 10^{-8}-1.0 \times 10^{-2}$ g/mL.

Light scattering measurements were conducted on an ALV/CGS-3 compact goniometer system (ALVGmbH, Germany), equipped with a ALV-5000/EPP multi-τ digital correlator with 288 channels and an ALV/LSE-5003 light-scattering electronics unit for stepper motor drive and limit switch control. A JDS Uniphase 22 mW He−Ne laser ($\lambda_0 = 632.8$ nm) was used as the light source. The details of LS theory can be found elsewhere.[30] Dynamic light scattering (DLS) experiments were carried out at scattering angles ranging from 20° to 150° to obtain the average hydrodynamic radius $\langle R_h \rangle$, hydrodynamic radius distribution $f(R_h)$, and polydispersity (PD = μ_2/Γ^2, where μ_2 is the second cumulant and Γ is the decay rate of the correlation function). PD and $f(R_h)$ acquired at the scattering angle of 90°, where the influence of dust was minimized, are shown in this paper. Apparent diffusion coefficient for a certain aggregate, D_{app}, was obtained by extrapolation to zero angle, which leads to apparent hydrodynamic radius, $\langle R_h \rangle$, via the Stokes−Einstein equation $R_h = k_B T/6\pi\eta_0 D$, where k_B, T, and η_0 are the Boltzmann constant, the absolute temperature, and the solvent viscosity, respectively. In static light scattering (SLS), the weight-average molar mass of the aggregates ($M_{w,agg}$), the *z*-average root-mean-square radius of gyration $\langle R_g^2 \rangle_z^{1/2}$ (or written as $\langle R_g \rangle$), and the second virial coefficient A_2 were obtained from the angular dependence of the absolute excess time-average scattering intensity, known as Rayleigh ratio $R_{vv}(q)$, on the basis of the Zimm plot

$$\frac{KC}{R_{vv}(q)} \cong \frac{1}{M_{w,agg}}\left(1+\frac{1}{3}\langle R_g^2\rangle q^2\right)+2A_2C$$

where $K = 4\pi^2 n^2 (dn/dC)^2/(N_A \lambda_0^4)$ and $q = (4\pi n/\lambda_0)\sin(\theta/2)$, with N_A, dn/dC, n, and λ_0 being the Avogadro number, the specific refractive index increment, the solvent refractive index, and the wavelength of the light in vacuum, respectively. The dn/dC value of each block−graft copolymer was estimated as the weighted average of PEO[31] and the backbone, using the compositions determined by ^{1}H NMR. The dn/dC of the backbone was assumed to be the dn/dC of PS in water.[31] It has to be noted that because of the low content of the backbone in the copolymer, the error coming from these estimations should be very small.

Results and Discussion

Synthesis of the Block−Graft Copolymers. The synthesis of PHOS and its block copolymers has been addressed before.[20,28,29] The molecular weights and compositions of the precursor copolymers for the backbones, PS-*b*-PtBOS, were determined by SEC and ^{1}H NMR. The fact that the observed molecular weights are close to the stoichiometric ones, together with the narrow molecular weight distributions, indicates the living nature of the polymerizations and the well-defined structure of the precursor block copolymers. The acidic hydrolysis removes the protecting *tert*-butoxy groups, creating phenolic groups (PhOH) on the backbone, and it has been proven to be quantitative.[28,29] The molecular weights and compositions of the final backbone diblock copolymers (Table 1), SHOS1 and SHOS2, have been calculated from the data of their respective precursors, taking into account the complete hydrolysis of *tert*-butoxy groups.

The grafting of EO was carried out in a manner similar to the procedures followed for the preparation of linear PEO, utilizing *t*-BuP_4 as a polymerization promoter.[24−26] Figure 1 gives the SEC traces of a typical block−graft copolymer before and after fractionation. The peak located at the higher elution volume is assigned to the linear PEO byproduct, which exists in every crude product regardless of the polymerization conditions and can be easily removed by fractionation. It is worth noting that these linear PEO byproducts, in all cases, have very low molecular weight distributions ($M_w/M_n < 1.05$), indicating that the polymerization leading

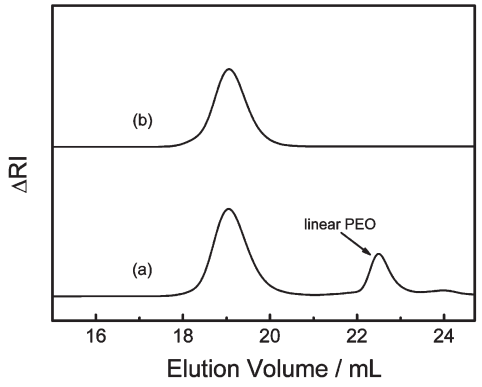

Figure 1. Size exclusion chromatography traces of a representative polystyrene-*block*-poly(*p*-hydroxystyrene-*graft*-ethylene oxide) copolymer (sample SHOS1gEO1) prepared via a combination of conventional and metal-free anionic polymerization: (a) crude reaction product before fractionation; (b) pure block−graft copolymer after solvent/nonsolvent fractionation.

to their preparation also has a controlled character. One possible explanation to the presence of linear PEO byproduct is that in each case not all *t*-BuP_4 molecules are protonated by the PhOH groups in the backbone. Some of them generate initiating sites with low-molecular-weight impurities, which probably come from the backbone or from *t*-BuP_4 itself (*t*-BuP_4 is a commercial reagent and was used after minimal purification since it is a solid), leading to the linear PEO.

Because of the high feed ratio of EO to the backbone in each case (Table 1), it is possible to estimate the weight fraction of EO monomer incorporated in the block−graft copolymer, f_g (Table 1), using the areas of the peaks in the SEC chromatograms, assigned to the block−graft copolymer and linear PEO, despite the difference in the refractive indexes of the backbone and PEO. Generally, a lower *t*-BuP_4/PhOH value results in a higher f_g. This may be, at least partially, because quantitative deprotonation of PhOH groups cannot be achieved due to the electrostatic repulsion,[20] especially at high *t*-BuP_4/PhOH ratio. The excess *t*-BuP_4 (not protonated by the PhOH groups in the backbone) can generate initiating sites with other impurities, resulting in linear PEO. However, with a lower *t*-BuP_4/PhOH, the excess of *t*-BuP_4 and the quantity of impurities coming from *t*-BuP_4 are less; thus, the amount of the initiating sites leading to the formation of linear PEO and the final content of linear PEO byproducts are reduced. This observation should be also related to changes in the equilibrium associated with the protonation of phosphazine base and possibly to intramolecular and intermolecular association effects involving the multifunctional macromolecular initiator. The molecular weight ($M_{w,cal}$) of each block−graft copolymer is calculated by f_g and the known molecular weight and composition of the corresponding backbone.

Figure 2 shows the SEC traces of all the block−graft copolymers after fractionation. Symmetric peaks and low polydispersities ($M_w/M_n < 1.10$, Table 1) were obtained for all the block−graft copolymers with SHOS1 as the backbone. However, for SHOS2, the polydispersity of the block−graft copolymer is relatively higher and the peak is less symmetric. A tailing is observed at the high elution volume part of the peak. Besides the fact that PEO with high molecular weight can possibly result in absorption of the polymer on the styragel SEC columns,[18] the solubility of the multifunctional initiator may also be the explanation.[24] Although both PS-*b*-PHOS copolymers, utilized as

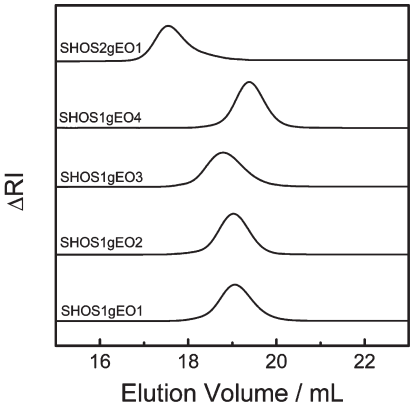

Figure 2. SEC traces of all the purified block−graft copolymers (after solvent/nonsolvent fractionation).

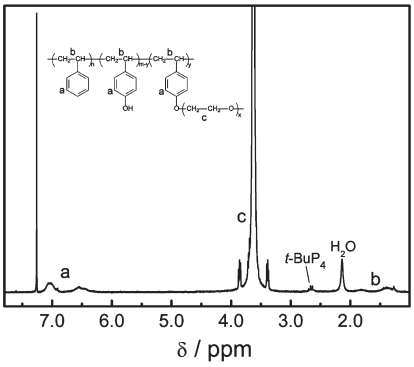

Figure 3. ^{1}H NMR spectrum of a representative PS-*b*-(PHOS-*g*-PEO) amphiphilic block−graft copolymer (sample SHOS1gEO1).

backbones, have good solubility in THF even at low temperature, it is obvious that after deprotonation by *t*-BuP_4, the polyoxyanions have a relatively poorer solubility. For SHOS2, the reaction solution becomes turbid upon mixing the backbone with *t*-BuP_4. The turbidity disappears ~2 h after the polymerization of EO starts at 45 °C. For SHOS1, slightly opaque solutions were observed when it was mixed with *t*-BuP_4. However, the solutions become clear and transparent only a few minutes after polymerization starts at 45 °C. The higher PS content and the lower overall molecular weight of SHOS1 lead to better solubility of the multifunctional initiator, so that good control of EO polymerization can be achieved from the initial stage of the polymerization reaction. A lower molecular weight distribution of the final product can be obtained in this case. It has to be noted that the value of *t*-BuP_4/PhOH should also be considered for the solubility of the initiator because it is the main factor that determines how many oxyanions are initially generated on the backbone. However, in our experiments, the influence of *t*-BuP_4/PhOH on the molecular weight distributions of the block−graft copolymers has not been manifested in a remarkable way.

Figure 3 presents the ^{1}H NMR spectrum of a typical block−graft copolymer after fractionation. All the characteristic peaks of PS and PEO can be observed. The molecular weight ($M_{w,NMR}$) of each block−graft copolymer is also determined by using the peak areas of aromatic protons in the backbone and methylene protons in PEO side chains. It can be seen in Table 1 that $M_{w,NMR}$ is systematically larger than $M_{w,cal}$. Except for the inherent errors in these two methods for the calculation of molecular weight, the most possible reason is that a certain amount of the block−graft

Table 2. Thermal Properties and Crystallinity of the Block−Graft Copolymers Obtained from DSC Measurements

sample	f_{PEO}[a] (%)	EO/PhOH[b]	$T_{m,PEO}$ (°C) (2nd cycle)	$X_{c,PEO}$ (%)
SHOS1gEO1	94.3	148	56.2	62.9
SHOS1gEO2	94.4	150	57.6	84.6
SHOS1gEO3	95.2	175	57.7	87.1
SHOS1gEO4	92.3	107	54.3	77.1
SHOS2gEO1	95.9	142	55.5	64.1

[a] Weight fraction of PEO in each block−graft copolymer calculated by $M_{w,NMR}$ (Table 1). [b] Molar ratio of EO to *p*-hydroxystyrene monomeric units in each block−graft copolymer, calculated by $M_{w,NMR}$ and the molecular characteristics of the backbone (Table 1).

copolymer with relatively lower molecular weight is removed during the fractionation, leaving a product with higher molecular weight ($M_{w,cal}$ was determined in the crude reaction product where $M_{w,NMR}$ was determined for the fractionated pure block−graft copolymers). It has to be noted that the signal coming from *t*-BuP_4 residue can also be observed even after two fractionations. This is because after the termination of the graft polymerization, *t*-BuP_4 exists in the protonated state and it is not easy to be removed completely in the fractionation step. However, the quantity of *t*-BuP_4 residue is calculated to be lower than 0.5 wt % in each of the final products. Therefore, it is assumed than such a low amount of *t*-BuP_4 does not influence the physical properties of the block−graft copolymers.

Making the assumption that the side chains of the block−graft copolymer have uniform length and molecular weight similar to that of the linear byproducts, we can get some information, at least to some extent, about the length of the side chains.[20] The molecular weight of the linear PEO byproducts, in all cases, is from 56 000 to 84 000 g/mol (apparent values from SEC without conversion to real values), so that most probably the PEO side chains are much longer than the backbone (for the SHOS1gEO series) or at least close to the length of the backbone (for sample SHOS2gEO1). Therefore, these block−graft copolymers must have a more starlike conformation.

Different values of *t*-BuP_4/PhOH were used for the graft polymerization of EO with SHOS1. It is somewhat surprising to see that even with *t*-BuP_4/PhOH being 0.2, well-defined block−graft copolymer can also be obtained. The time of the graft polymerization was set to 48 h to ensure full conversion of EO monomer in all cases. Unfortunately, we could not take out samples by flame sealing appropriate constrictions in the polymerization apparatus during the polymerization, in order to study the kinetics, because heating may cause pyrolysis of THF into products that can cause damage to the polymerization reaction.[32]

Thermal Properties of the Block−Graft Copolymers. DSC measurements were implemented in order to get some information mainly on the crystallization behavior of the block−graft copolymers synthesized under different experimental conditions and possibly extracting some picture regarding their macromolecular architecture. Table 2 lists the melting temperature, $T_{m,PEO}$ (endothermic maximum, in the second cooling−heating cycle), and crystallinity ($X_{c,PEO}$) of PEO side chains in different block−graft copolymer samples. The glass transition temperature (T_g) of PS cannot be differentiated in any of the DSC thermograms because of the low content of the backbone in all cases. Moreover, T_g of PEO will not be discussed here because the glass transition of PEO side chains is also not visible in the thermograms due most probably to the relatively high crystallinity of the samples.[33] $X_{c,PEO}$ is calculated as the ratio of measured melting enthalpy per gram of PEO in each sample to the heat of fusion of 100% crystalline PEO (200 J/g).[34] $T_{m,PEO}$ remains relatively constant (55.5 ± 2.5 °C) for all samples (Table 2). However, the differences in $X_{c,PEO}$ are much more remarkable. $X_{c,PEO}$ is known to rise with the increase in the overall content of PEO and the length of PEO side chains in the graft copolymer.[33,35−37] Since the weight fractions of PEO (f_{PEO}) in the present block−graft copolymers are close to each other (Table 2), the differences in $X_{c,PEO}$ can be attributed mostly to the length of PEO side chains, which should be influenced by the experimental conditions for the graft polymerization.

In order to make better comparisons, the ratio between EO and *p*-hydroxystyrene monomeric units or phenolic groups (EO/PhOH) is shown for each case. For SHOS1gEO series, it is not surprising to see that SHOS1gEO3, which has the highest EO/PhOH, presents the highest $X_{c,PEO}$. However, SHOS1gEO1, which has a value of EO/PhOH close to that of SHOS1gEO2 and higher than that of SHOS1gEO4, shows the lowest $X_{c,PEO}$. The shortest PEO side chains seem to be present in SHOS1gEO1.

It seems to us that a higher *t*-BuP_4/PhOH (Table 1) for the graft polymerization results in higher grafting densities and shorter PEO side chains. The polymerization of ethylene oxide with phenol in the presence of *t*-BuP_4 has been studied by Schlaad et al.[25] for the synthesis of linear PEO. The ratio of *t*-BuP_4 to phenol was 1.0; molecular weights close to stoichiometric ones were obtained (initiation efficiency close to 1). Additionally, Antonietti et al.[26] utilized 0.5 equiv of *t*-BuP_4 to hydroxyl groups and also synthesized well-defined linear PEO. These results constitute convincing evidence that the reaction between the propagating alkoxide and the residual hydroxyl groups does exist, and the length of the side chains tends to be uniform due to this mechanism, even when the ratio of *t*-BuP_4 to hydroxyl group is lower than one. However, for the macromolecular multifunctional initiating and propagating system, the situation should be much more complicated due to both intramolecular and intermolecular hydrogen abstraction and the hydrogen abstraction between the end groups on the side chains of the graft copolymer and the end groups on the linear PEO byproducts. Therefore, our initial expectation is that the overall protonation−deprotonation equilibrium involving the living ends and the counterions would result in the same molecular architecture even though the value of *t*-BuP_4/PhOH changes, which is different from the results reflected by DSC.

Two kinetic reasons are proposed here: (a) *t*-BuP_4 is such a strong base[25,38] that, once protonated, it does not readily release the proton back into the proton equilibrium. (b) It is possible for the alkoxide living ends to abstract the protons of the PhOH groups, which are not deprotonated by *t*-BuP_4 in the first place.[20] However, this proton abstraction becomes more and more difficult as the side chains grows, especially when lower *t*-BuP_4/PhOH is used, leaving some *p*-hydroxystyrene monomeric units not grafted with PEO. Therefore, lower *t*-BuP_4/PhOH leads to lower grafting density and longer PEO side chains taking into account the values of EO/PhOH. Nevertheless, it is still difficult to discuss this point in a more quantitative manner because it is difficult to determine the amount of *t*-BuP_4 that participates in the deprotonation of the PhOH groups in the backbone, and the degree of the further proton abstraction is also undeterminable.

SHOS2gEO1 was synthesized by utilizing a lower *t*-BuP_4/PhOH ratio (compared to SHOS1gEO1) and has a higher EO/PhOH (compared to SHOS1gEO4). However, this block−graft copolymer also has a relatively lower value of $X_{c,PEO}$. This should be attributed to the longer backbone and higher content of PHOS in the backbone,

which prevent the PEO side chains from organizing into a higher degree.[33,35−37]

Solution Properties of the Amphiphilic Block−Graft Copolymers. All the block−graft copolymers derived from diblock SHOS1 are readily soluble in water, and the stock solutions of them were prepared by dissolving the solid samples directly in water (at 60 °C overnight to ensure complete dissolution). However, SHOS2gEO1, which has a much longer PS segment, is not soluble in water even upon heating or after sonication. Therefore, the THF−water protocol (as described in the Experimental Section) had to be employed in order to dissolve the particular sample into water.

The critical micelle concentrations (cmc) for all the block−graft copolymer samples have been determined by aid of fluorescence spectroscopy.[39,40] A typical plot of I_1/I_3 ratio vs copolymer concentration is shown in Figure 4. The downward turning of the I_1/I_3 vs C plot at the low concentration region clearly indicates that aggregation does exist in the system, despite the low content of the hydrophobic backbone in the block−graft copolymer (Table 3). The cmc values determined from the inflection point of the I_1/I_3 ratio vs C at the low concentration region are listed in Table 3. The main reason for making experiments and a discussion on cmc is to present evidence for the micellization of the block−graft copolymers (the existence of a cmc is related to the formation of micelles in the system). The cmc values of all the block−graft copolymers are not so different (around $\sim 1.0 \times 10^{-5}$ g/mL in all cases, due to the similar content of hydrophobic backbones in the copolymers), and the differences are probably within the experimental error of the method. These cmc values are about 1 order of magnitude higher than the linear PS−PEO amphiphilic block copolymers,[39,40] which should be attributed to the high content of PEO and the starlike macromolecular structure of the block−graft copolymers.

An interesting observation is the existence of pyrene excimer fluorescence in the solutions of a certain sample. For the SHOS1gEO series, only the emission of pyrene "monomer" (360−420 nm) is observed even at the highest copolymer concentration investigated (1 wt %). However, for SHOS2gEO1, the broad emission of pyrene excimer[41−43] (ca. 470 nm) is observed when the copolymer concentration is higher than its cmc. For the purpose of a better comparison, the fluorescence emission spectra of pyrene in the presence of SHOS2gEO1 and a typical SHOS1gEO block−graft copolymer at the same concentration (1.0×10^{-4} g/mL) are shown in Figure 5. The intensity of the excimer emission rises as the concentration of SHOS2gEO1 increases (not shown). This observation reveals that in the aggregates formed by the SHOS1gEO samples compact hydrophobic domains do not exist, probably because of the high content of the hydrophilic PEO side chains and the starlike molecular structure of the block−graft copolymers. However, in the SHOS2gEO1 aggregates, regardless of the molecular composition and architecture, the much longer PS segments have the ability to form more compact hydrophobic domains with low microviscosity, which forces the probes to be close enough to each other and to form excimers.[41−43] This is also evidenced by the difference in the value of I_1/I_3 ratios at high copolymer concentrations. For all samples of the SHOS1gEO series, the I_1/I_3 ratio decreases eventually to a plateau at ca. 1.45 for concentrations higher than cmc. This value is much higher than that for linear PS−PEO block copolymers (which is usually lower than 1.2),[39,40] indicating that the interior environment of SHOS1gEO aggregates is not so hydrophobic. However, for sample SHOS2gEO1, the I_1/I_3 ratio drops to 1.17 at the highest concentration investigated, which gives further evidence that compact hydrophobic domains exist in these aggregates formed by the block−graft copolymer with a long PS hydrophobic segment.

The micellar aggregates formed by the amphiphilic block−graft copolymers were further characterized by light scattering. The structural parameters of the micellar

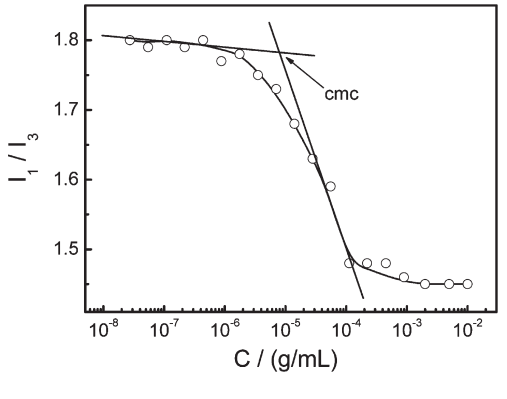

Figure 4. Plot of the intensity ratio (I_1/I_3) in the pyrene fluorescence emission spectrum as a function of copolymer concentration for aqueous solutions of sample SHOS1gEO4.

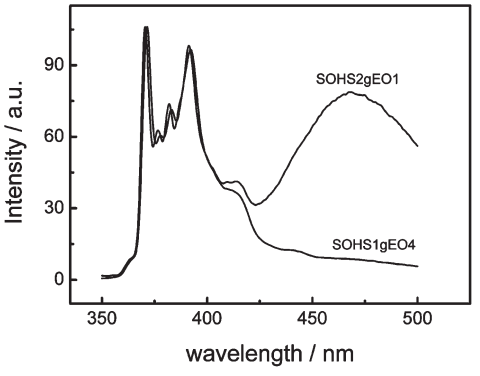

Figure 5. Fluorescence emission spectra of pyrene in water (2.7×10^{-7} M) in the presence of SHOS2gEO1 and SHOS1gEO4 block−graft copolymers, where the copolymer concentration is similar in both cases ($C = 1.0 \times 10^{-4}$ g/mL).

Table 3. Solution Properties of the Block−Graft Copolymers in Water, As Determined from Fluorescence Spectroscopy and Light Scattering Measurements

sample	f_b[a] (%)	cmc × 10^5 (g/mL)	$M_{w,agg}$[b] × 10^{-6} (g/mol)	A_2[b] × 10^5 (mol mL/g^2)	N_{agg}	$\langle R_h \rangle$[c] (nm)	PD[d]	$\langle R_g \rangle / \langle R_h \rangle$[c]	d_{agg} (g/mL)
SHOS1gEO1	5.7	1.34	2.62	1.36	8.3	26.6	0.102	1.11	0.056
SHOS1gEO3	4.8	1.39	2.30	1.51	6.2	25.0	0.083	1.08	0.059
SHOS1gEO4	7.7	0.79	2.46	0.82	10.5	24.5	0.096	0.99	0.067
SHOS2gEO1	4.1	1.14	13.4	1.96	11.5	53.4	0.132	1.17	0.036

[a] Weight fraction of the backbone in the block−graft copolymer. [b] Obtained from Zimm plot for each block−graft copolymer sample in water. [c] The values for the radii utilized are the ones obtained after extrapolation to zero angle and zero concentration. [d] The values of polydispersity are those obtained at 90° and at a concentration of ca. 3.0×10^{-4} g/mL.

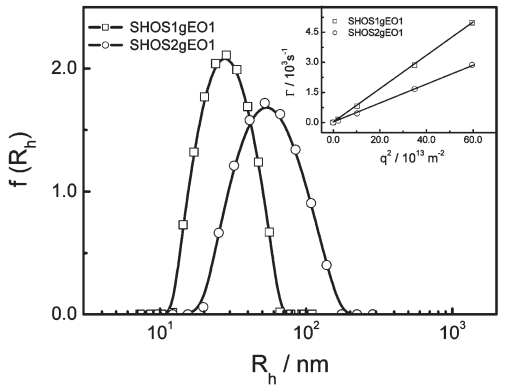

Figure 6. Hydrodynamic radius distribution, $f(R_h)$, at 90° of the micellar aggregates formed by samples SHOS2gEO1 and SHOS1gEO1 at the same concentration of the block−graft copolymer ($C = 3.0 \times 10^{-4}$ g/mL) in water. Inset: scattering vector (q) dependence of average line width (Γ) for the corresponding micellar aggregates.

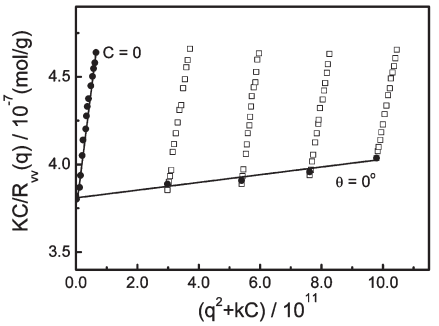

Figure 7. Zimm plot for the micellar aggregates formed by sample SHOS1gEO4 in water.

aggregates are listed in Table 3. The sizes of the micellar aggregates formed by the samples of the SHOS1gEO series are very close to each other, while the SHOS2gEO1 aggregates have a much larger $\langle R_h \rangle$. This should be due to the different length of the backbones, which is the main factor contributing to the $\langle R_h \rangle$ of the aggregates in this case. However, a direct comparison between copolymer SHOS2gEO1 and the rest of the samples cannot be made due to the use of a different micelle preparation protocol for the particular copolymer. The micellar aggregates have relatively low polydispersities and unimodal hydrodynamic radius distributions (Figure 6). The linear dependence of Γ to q^2 (inset of Figure 6) implies that these aggregates are isotropically diffusing species.

$M_{w,agg}$, $\langle R_g \rangle$, and A_2 for the micellar aggregates are obtained from the corresponding Zimm plots (Figure 7) constructed for each block−graft copolymer in aqueous solutions. The aggregation number N_{agg} of the micellar aggregates is calculated as $M_{w,agg}/M_{w,NMR}$, where $M_{w,NMR}$ is the molecular weight of each block−graft copolymer (Table 1). The overall density (d_{agg}) of the aggregates has been calculated as $d_{agg} = M_{w,agg}/(4/3\pi\langle R_h \rangle^3 N_A)$, assuming that the aggregates have spherical structures. Despite the low content of the hydrophobic backbone, the second virial coefficient, A_2, obtains relatively low values for the block−graft copolymers, indicating that water is still a highly selective solvent. The values of $\langle R_g \rangle/\langle R_h \rangle$ (found in the range 0.99−1.17 for the amphiphilic block−graft copolymer in water) present good evidence that these micellar aggregates have a structure similar to hyperbranched clusters[44] due to the starlike molecular architecture of the unimers. Because of the high content of the hydrophilic PEO side chains, the aggregates are expected to be highly swelled with low d_{agg} and low N_{agg}, as experimental results indicate.

Conclusions

PS-*b*-(PHOS-*g*-PEO) block−graft copolymers have been successfully synthesized by following a novel synthetic approach involving the combination of conventional and metal-free anionic polymerization and postpolymerization functionalization. The PEO side chains are synthesized by the "grafting-from" technique via metal-free anionic polymerization, using *t*-BuP_4 and the phenolic hydroxyl groups on the backbone of the PS-*b*-PHOS diblock copolymers, in order to generate the multifunctional initiating system. The combined results from SEC, ^{1}H NMR, and DSC have supported the idea that with different values of *t*-BuP_4/PhOH, block−graft copolymers with different molecular characteristics can be prepared. Generally, lower *t*-BuP_4/PhOH leads to lower grafting density and longer PEO side chains, taking into account the ratio of ethylene oxide and *p*-hydroxystyrene repeating units as well. The fluorescence and light scattering studies have revealed that the amphiphilic block−graft copolymers form highly swelled micellar aggregates in water, with low aggregation numbers and supramolecular structure resembling that of hyperbranched clusters. Compact hydrophobic domains only exist in the micellar aggregates formed by the block−graft copolymer with a long PS hydrophobic block.

Acknowledgment. J.Z. thanks the China Scholarship Council for offering the scholarship to work in TPCI-NHRF, Greece.

References and Notes

(1) Neugebauer, D. *Polym. Int*. **2007**, *56*, 1469–1498.
(2) Xie, H.-Q.; Xie, D. *Prog. Polym. Sci*. **1999**, *24*, 275–313.
(3) (a) Ali, M. M.; Stöver, H. D. H. *Macromolecules* **2004**, *37*, 5219–5227. (b) Luz, J.-F.; Hoth, A. *Macromolecules* **2006**, *39*, 893–896. (c) Hester, J. F.; Banerjee, P.; Won, Y.-Y.; Akthakul, A.; Acar, M. H.; Mayes, A. M. *Macromolecules* **2002**, *35*, 7652–7661. (d) Ishizone, T.; Han, S.; Hagiwara, M.; Yokoyama, H. *Macromolecules* **2006**, *39*, 962–970. (e) Xu, J.-T.; Ji, J. *Polymer* **2003**, *44*, 6379–6385. (f) Neugebauer, D.; Zhang, Y.; Pakula, T.; Sheiko, S. S.; Matyjaszewski, K. *Macromolecules* **2003**, *36*, 6746–6755. (g) Yokoyama, H.; Miyamae, T.; Han, S.; Ishizone, T.; Tanaka, K.; Takahara, A.; Torikai, N. *Macromolecules* **2005**, *38*, 5180–5189.
(4) (a) Xu, P.; Tang, H.; Li, S.; Ren, J.; Van Kirk, E.; Murdoch, W. J.; Radosz, M.; Shen, Y. *Biomacromolecules* **2004**, *5*, 1736–1744. (b) Robinson, D. N.; Peppas, N. A. *Macromolecules* **2002**, *35*, 3668–3674. (c) Li, X.; Ji, J.; Shen, J. *Polymer* **2006**, *47*, 1987–1994. (d) Zhang, R.; Seki, A.; Ishizone, T.; Yokoyama, H. *Langmuir* **2008**, *24*, 5527–5533. (e) Oyane, A.; Ishizone, T.; Uchida, M.; Furukawa, K.; Ushida, T.; Yokoyama, H. *Adv. Mater*. **2005**, *17*, 2329–2332.
(5) (a) Forder, C.; Patrickios, C. S.; Armes, S. P.; Billingham, N. C. *Macromolecules* **1996**, *29*, 8160–8169. (b) Aoshima, S.; Sugihara, S. *J. Polym. Sci., Part A: Polym. Chem*. **2000**, *38*, 3962–3965.
(6) (a) Ishizone, T.; Han, S.; Okuyama, S.; Nakahama, S. *Macromolecules* **2003**, *36*, 42–49. (b) Han, S.; Hagiwara, M.; Ishizone, T. *Macromolecules* **2003**, *36*, 8312–8319. (c) Ishizone, T.; Seki, A.; Hagiwara, M.; Han, S.; Yokoyama, H.; Oyane, A.; Deffieux, A.; Carlotti, S. *Macromolecules* **2008**, *41*, 2963–2967.
(7) (a) Rieger, J.; Bernaerts, K. V.; Du Prez, F. E.; Jérôme, R.; Jérôme, C. *Macromolecules* **2004**, *37*, 9738–9745. (b) Riger, J.; Dubois, P.; Jérôme, R.; Jérôme, C. *Langmuir* **2006**, *22*, 7471–7479.
(8) (a) Breitenkamp, K.; Simeone, J.; Jin, E.; Emrick, T. *Macromolecules* **2002**, *35*, 9249–9252. (b) Chemtob, A.; Hroguez, V.; Gnanou, Y. *Macromolecules* **2002**, *35*, 9262–9269.
(9) (a) Qiu, X.; Wu, C. *Macromolecules* **1997**, *30*, 7921–7926. (b) Laukkanen, A.; Winnik, F. M.; Tenhu, H. *Macromolecules* **2005**, *38*, 2439–2448.
(10) Wang, Y.; Huang, J. *Macromolecules* **1998**, *31*, 4057–4060.
(11) (a) Cheng, Z.; Zhu, X.; Fu, G. D.; Kang, E. T.; Neoh, K. G.; Wang, Y.; Huang, J. *Macromolecules* **2005**, *38*, 7187–7192. (b) Cheng, Z.; Zhu, X.; Kang, E. T.; Neoh, K. G. *Langmuir* **2005**, *21*, 7180–7185.

(12) (a) Wang, X. −S.; Lascelles, S. F.; Jackson, R. A.; Armes, S. P. *Chem. Commun.* **1999**, 1817–1818. (b) Wang, X.-S.; Armes, S. P. *Macromolecules* **2000**, *33*, 6640–6647. (c) Robinson, K. L.; de Paz-Báñez, M. V.; Wang, X. S.; Armes, S. P. *Macromolecules* **2001**, *34*, 5799–5805.
(13) (a) Neugebauer, D.; Zhang, Y.; Pakula, T.; Matyjaszewski, K. *Macromolecules* **2005**, *38*, 8687–8693. (b) Neugebauer, D.; Rydz, J.; Geobel, I.; Dacko, P.; Kowalczuk, M. *Macromolecules* **2007**, *40*, 1767–1773.
(14) Dérand, H.; Wesslén, B.; Wittgren, B.; Wahlund, K.-G. *Macromolecules* **1996**, *29*, 8770–8775.
(15) (a) Virtanen, J.; Baron, C.; Tenhu, H. *Macromolecules* **2000**, *33*, 336–341. (b) Virtanen, J.; Tenhu, H. *Macromolecules* **2000**, *33*, 5970–5975.
(16) Yuan, W.; Yuan, J.; Zhang, F.; Xie, X.; Pan, C. *Macromolecules* **2007**, *40*, 9094–9102.
(17) Lanson, D.; Schappacher, M.; Borsali, R.; Deffieux, A. *Macromolecules* **2007**, *40*, 9503–9509.
(18) Gauthier, M.; Tichagwa, L.; Downey, J. S.; Gao, S. *Macromolecules* **1996**, *29*, 519–527.
(19) Njikang, G. N.; Gao, L.; Gauthier, M. *Langmuir* **2008**, *24*, 12919–12927.
(20) Se, K.; Miyawaki, K.; Hirahara, K.; Takano, A.; Fujimoto, T. *J. Polym. Sci., Part A: Polym. Chem.* **1998**, *36*, 3021–3034.
(21) Kamber, N. E.; Jeong, W.; Waymouth, R. M. *Chem. Rev.* **2007**, *107*, 5813–5840.
(22) Förster, S.; Krämer, E. *Macromolecules* **1999**, *32*, 2783–2785.
(23) (a) Pispas, S.; Hadjichristidis, N. *Langmuir* **2003**, *19*, 48–54. (b) Pispas, S. *J. Polym. Sci., Part A: Polym. Chem.* **2006**, *44*, 606–613.
(24) Esswein, B.; Steidl, N. M.; Möller, M. *Macromol. Rapid Commun.* **1996**, *17*, 143–148.
(25) Schlaad, H.; Kukula, H.; Rudloff, J.; Below, I. *Macromolecules* **2001**, *34*, 4302–4304.
(26) Groenewolt, M.; Brezesinski, T.; Schlaad, H.; Antonietti, M.; Groh, P. W.; Iván, B. *Adv. Mater.* **2005**, *17*, 1158–1162.
(27) (a) Hadjichristidis, N.; Iatrou, H.; Pispas, S.; Pitsikalis, M. *J. Polym. Sci., Part A: Polym. Chem.* **2000**, *38*, 3211–3234. (b) Uhrig, D.; Mays, J. W. *J. Polym. Sci., Part A: Polym. Chem.* **2005**, *43*, 6179–6222.
(28) Mountrichas, G.; Mantzaridis, C.; Pispas, S. *Macromol. Rapid Commun.* **2006**, *27*, 289–294.
(29) Mountrichas, G.; Pispas, S. *Macromolecules* **2006**, *39*, 4767–4774.
(30) (a) Huglin, M. B., Ed. *Light Scattering from Polymer Solutions*; Academic: New York, 1972. (b) Teraoka, I. *Polymer Solutions*; John Wiley & Sons: New York, 2002. (c) Berne, B. J.; Pecora, R. *Dynamic Light Scattering*; Plenum Press: New York, 1976. (d) Chu, B. *Laser Light Scattering*, 2nd ed.; Academic Press: New York, 1991.
(31) *Polymer Handbook*, 3rd ed.; Brandup, J., Immergut, E. H., Eds.; Wiley-Interscience: New York, 1989.
(32) Ekizoglou, N.; Hadjichristidis, N. *J. Polym. Sci., Part A: Polym. Chem.* **2001**, *39*, 1198–1202.
(33) Li, L.; Zheng, S. *J. Polym. Sci., Part B: Polym. Chem.* **2008**, *46*, 2296–2306.
(34) Floudas, G.; Ulrico, R.; Wiesner, U. *J. Chem. Phys.* **1999**, *110*, 652–663.
(35) Cianga, L.; Sarac, A.; Ito, K.; Yagci, Y. *J. Polym. Sci., Part A: Polym. Chem.* **2005**, *43*, 479–492.
(36) Jannasch, P.; Wesslén, B. *J. Polym. Sci., Part A: Polym. Chem.* **1995**, *33*, 1465–1474.
(37) Zhang, W.; Shiotsuki, M.; Masuda, T. *Macromolecules* **2007**, *40*, 1421–1428.
(38) Schweisinger, R.; Hasenfratz, C. *Angew. Chem.* **1993**, *105*, 1420–1422.
(39) Zhao, C.-L.; Winnik, M. A.; Riess, G.; Croucher, M. D. *Langmuir* **1990**, *6*, 514–516.
(40) Wilhelm, M.; Zhao, C.-L.; Wang, Y.; X, R.; Winnik, M. A.; Mura, J.-L.; Riess, G.; Croucher, M. D. *Macromolecules* **1991**, *24*, 1033–1040.
(41) (a) Nivaggioli, T.; Alexandridis, P.; Hatton, T. A.; Yekata, A.; Winnik, M. A. *Langmuir* **1995**, *11*, 730–737. (b) Nivaggioli, T.; Tsao, B.; Alexandridis, P.; Hatton, T. A. *Langmuir* **1995**, *11*, 119–126.
(42) Winnik, F. M. *Macromolecules* **1990**, *23*, 233–242.
(43) Yekta, A.; Duhamel, J.; Brochard, P.; Adiwidjaja, H.; Winnik, M. A. *Macromolecules* **1993**, *26*, 1829–1836.
(44) (a) Burchard, W. In *Light Scattering Principles and Development*; Brown, W., Ed.; Clarendon Press: Oxford, 1996; p 439. (b) Burchard, W.; Schmidt, M.; Stockmayer, W. H. *Macromolecules* **1980**, *13*, 1265–1272.